NASA Precipitation Measurement Missions
(PMM) Science Team Meeting

1-4 November 2010
Seattle, WA, USA

Orographic Precipitation Processes and High-Resolution Hydrometeorological Modeling in the Southern Appalachians

Ana P. Barros, Xiaoming Sun, Anna Wilson, Jing Tao, Douglas Miller*, and Olivier Prat
Duke University, *UNC-Asheville

1. Interannual variability of orographic rainfall

The current configuration of the PMM hydrometeorological network in the Appalachians including 32 raingauge stations and one flux tower was completed in 2009 (Fig.1.1).

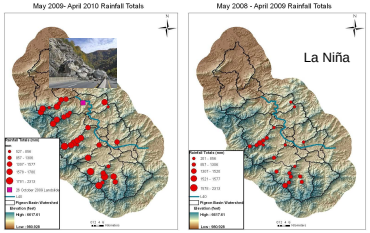

Annual amounts in 09-10 (strong EL Niño) compared against annual amounts in 08-09 (moderate to weak La Niña) show an increase in annual rainfall of about **50%**.

Significant increases take place in the months of May, September (Figs 1.2a and b) and December.

Fig. 1.1: *Spatial distribution of annual precipitation totals. The landslide in October 2009 Was responsible for keeping I-40 closed for months.*

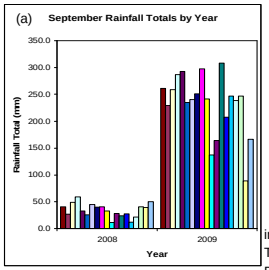

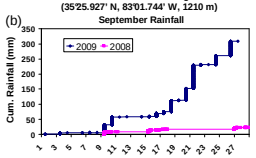

Fig. 1.2: *a) September rainfall totals in 2008 and 2009; b) cumulative rainfall curves.*

The data show that **the difference is** not in number of storms, but **in storm intensity**. This result is contradicts previous climatology Derived without high elevation data.

2. Evaluation of Satellite Products

2.1 QPE Adjustment

A data base of optimal QPE is being derived from NSSL's Q2 product by applying an orographic adjustment based on the PMM raingauge network at high elevations as well as valley stations from the HADS and ECOnet networks at low elevations (method 2), and without any separation by elevation threshold (method 1). Though differences in RMSE are small between the methods, there is marked improvement in low elevation QPE using method 2 (Fig.2.1).

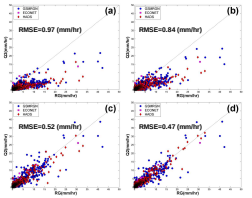

Fig. 2.1: *a) Q2RAD_HSR; b) 2RAD_HSR_GC, and Adjusted c) Q2RAD_HSR_GC_M1; d) Q2RAD_HSR_GC_M2.*

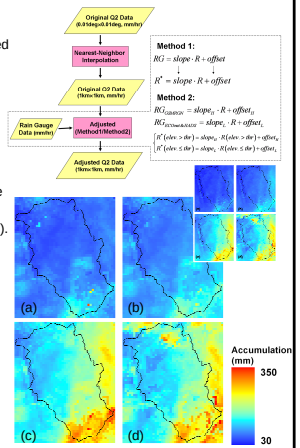

Fig. 2.2: *Monthly precipitation during August 2008.Top right corner inset shows total rainfall for tropical storm Fay. (a-d) as in Fig. 2.1.*

2.2 TRMM PR 2A25

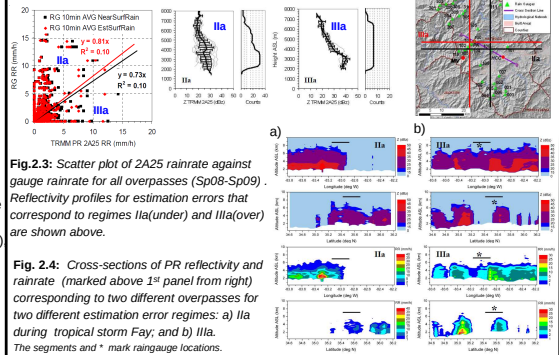

Fig.2.3: *Scatter plot of 2A25 rainrate against gauge rainrate for all overpasses (Sp08-Sp09) . Reflectivity profiles for estimation errors that correspond to regimes IIa(under) and IIIa(over) are shown above.*

Fig. 2.4: *Cross-sections of PR reflectivity and rainrate (marked above 1st panel from right) corresponding to two different overpasses for two different estimation error regimes: a) IIa during tropical storm Fay; and b) IIIa.*
*The segments and * mark raingauge locations.*

3. Dynamical downscaling and related uncertainties

To understand the mechanisms associated with the spatial and temporal rainfall distribution over the Southern Appalachians high resolution down to 1 km resolution dynamical downscaling of Hurricane Ivan, 2004 was conducted using WRF3.1.

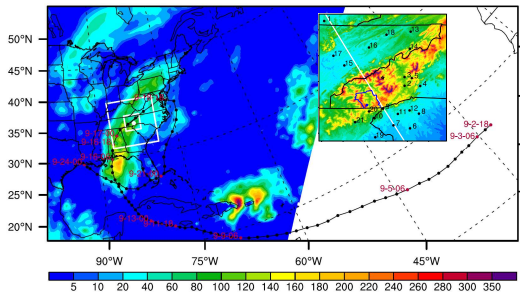

Fig. 3.1: The best track of Hurricane Ivan and the NARR rainfall accumulation from 0600 UTC, September 15 to 0600 UTC, September 18, 2004. The two white grids indicate the outer and inner domains of this study. Inset is a zoom of domain 2.

3.1 Orographic effects on spatial structure

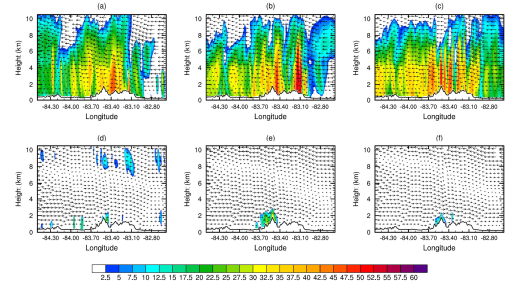

Fig. 3.2: *Radar reflectivity (dBz) along the cross section shown in Fig. 3.1 at 5pm, 7pm and 9pm EST of September 16 (a to c) and 17 (d to f), 2004 from NARR_YSU.*

3.2 Downscaled rainfall in the inner mountain region

Table 3.1: Simulation configurations and physics options.

Simulation	Horizontal Resolution	Grid Cells	MP	LR	SR	LSM	PBL	SL	Cumulus
NARR_YSU	3km (D01), 1km (D02)	271x271x35	Lin et al.	RRTM	Dudhia	Noah	YSU	MM5	NA
NARR_MYJ	3km (D01), 1km (D02)	271x271x35	Lin et al.	RRTM	Dudhia	Noah	MYJ	MYJ	NA
NARR_Cumu	3km (D01), 1km (D02)	271x271x35	Lin et al.	RRTM	Dudhia	Noah	YSU	MM5	KF
NARR_woTopo	3km (D01), 1km (D02)	271x271x35	Lin et al.	RRTM	Dudhia	Noah	YSU	MM5	NA

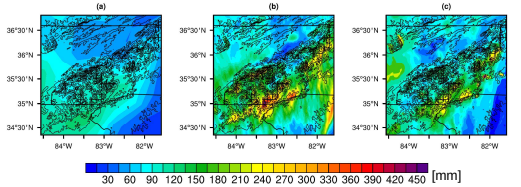

Fig. 3.3: *Accumulative precipitation from (a) NARR, (b) NARR_YSU downscaling, and NCEP Stage IV observations.*

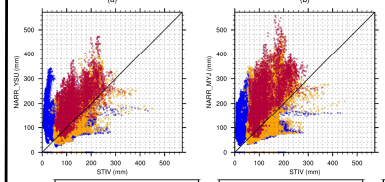

Fig. 3.4: *Scatter plot of accumulated rainfall of each grid cell for: (a) NCEP Stage IV vs. NARR_YSU and (b) NCEP Stage IV vs. NARR_MYJ.*

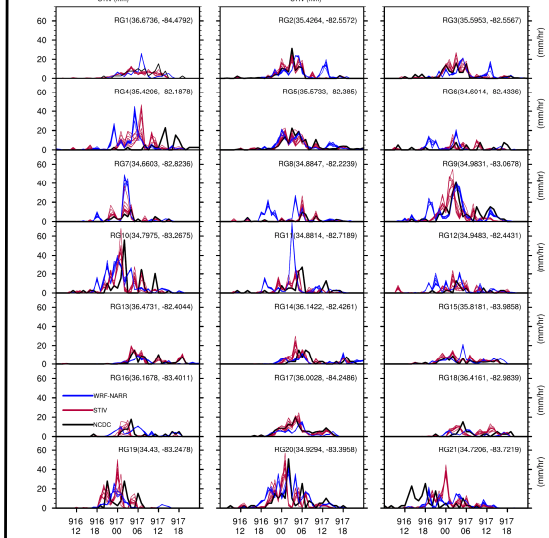

Fig. 3.5: *Hourly rainfall time series of each NCDC station documented in Fig. 3.1 and the retrieved rainfall time series from NCEP Stage IV (red) and NARR3Hrly_YSU (blue).*

3.4 Sensitivity to model configuration

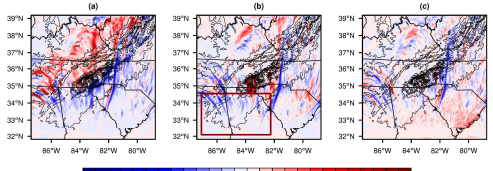

Fig. 3.6: *Differences of accumulated rainfall between NARR_YSU and a) NARR_woTopo, b) NARR_MYJ, c) NARR_Cumu. The small rectangle in (b) is the region used for horizontal average in Fig. 3.7; and the large rectangle is for Fig. 3.8.*

NARR-MYJ simulates heavier orographic rainfall at high elevation over steep terrain (see also Fig. 3.4). Deep convection is more developed in the NARR-YSU.

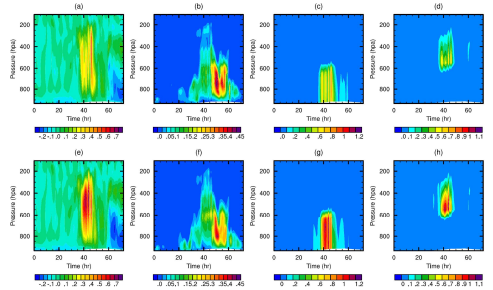

Fig. 3.7: *Time evolution of horizontally averaged vertical wind velocity (m/s), cloud water plus cloud ice (g/kg), rain water (g/kg), and snow plus graupel (g/kg) for NARR_YSU (a to d) and NARR_MYJ (e to h) in the southwest corner of domain 1.*

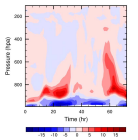

Fig. 3.8: *Differences of horizontally averaged RH between NARR_YSU and NARR_MYJ in the southwest corner of domain 1 (see Fig. 3.6b).*

$$\frac{\partial T}{\partial t} = -\vec{V}\cdot\vec{\nabla}T - w\frac{\partial T}{\partial z} + \frac{\kappa T}{P}\left(\frac{\partial P}{\partial t} + \vec{V}\cdot\vec{\nabla}P + w\frac{\partial P}{\partial z}\right) + \frac{J}{c_p} \qquad \text{(Eq. 3.1)}$$

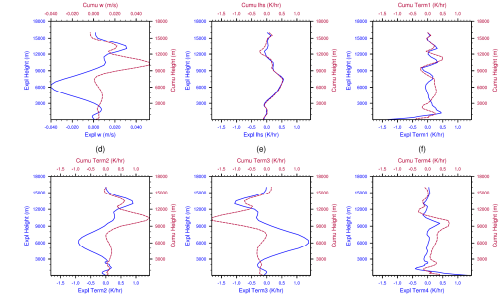

Fig. 3.9: *Vertical profile of (a) vertical wind velocity (m/s) and (b) temperature tendency (K/hour) by (c) term 1, (d) term 2, (e) term 3 and (f) term 4 of Eq.(3.1) at 1800 UTC, September 16, 2004 over grid points with and without parameterized cumulus rainfall in the past 10 min in domain 1.*